ORIGINAL RESEARCH

Dual-layer aligned-random nanofibrous scaffolds for improving gradient microstructure of tendon-to-bone healing in a rabbit extra-articular model

Jiangyu Cai,[1,*] Juan Wang,[2,*]
Kaiqiang Ye,[2] Dandan Li,[2]
Chengchong Ai,[1] Dandan
Sheng,[1] Wenhe Jin,[1]
Xingwang Liu,[1] Yunlong
Zhi,[1] Jia Jiang,[1] Jun Chen,[1,3,4]
Xiumei Mo,[2] Shiyi Chen[1]

[1]Department of Sports Medicine,
Huashan Hospital, Fudan University,
Shanghai 200040, China; [2]State
Key Laboratory for Modification
of Chemical Fibers and Polymer
Materials, College of Chemistry,
Chemical Engineering and
Biotechnology, Donghua University,
Shanghai 201620, China; [3]Shanghai
BJ-KMC Medical Technology Co., Ltd,
Shanghai 201707, China; [4]State Key
Laboratory of Molecular Engineering
of Polymers, Fudan University,
Shanghai 200433, China

*These authors contributed equally
to this work

Correspondence: Xiumei Mo
State Key Laboratory for Modification of
Chemical Fibers and Polymer Materials,
College of Chemistry, Chemical
Engineering and Biotechnology, Donghua
University, Shanghai 201620, China
Tel +86 21 6779 2653
Email xmm@dhu.edu.cn

Shiyi Chen
Department of Sports Medicine, Huashan
Hospital, Fudan University, 12 Middle
Wulumuqi Road, Shanghai 200040, China
Tel +86 21 5288 8255
Email cshiyi@163.com

Background: Tendon/ligament injuries are common sports injuries. Clinically, the repair of a ruptured tendon or ligament to its bony insertion is needed, but the enthesis structure is not well reestablished following surgical repair. Herein, we fabricated dual-layer aligned-random scaffold (ARS) by electrospinning and aimed to investigate the effect of the scaffold on tendon-to-bone healing in vivo.

Materials and methods: The random and dual-layer aligned-random silk fbroin poly(L-lactic acid-co-e-caprolactone) (P(LLA-CL)) nanofibrous scaffolds were successfully fabricated by electrospinning methods. Ninety New Zealand white rabbits were randomly divided into three groups (random scaffold [RS], ARS, and control groups), and they were subjected to surgery to establish an extra-articular tendon-to-bone healing model with autologous Achilles tendon.

Results: Histological assessment showed that the ARS significantly increased the area of metachromasia, decreased the interface width, and improved collagen maturation and organization at the tendon–bone interface compared with the RS and control groups. Microcomputed tomography analysis showed that the bone tunnel area of RS and ARS groups was significantly smaller than those of the control group. Real-time polymerase chain reaction showed that BMP-2 and osteopontin expression levels of the tissue at the interface between the bone and graft in the RS and ARS groups were higher than those of the control group at 6 weeks. Collagen I expression level of the ARS group was significantly higher than those of the RS and control groups at 6 and 12 weeks. Moreover, the ARS groups had a better ultimate load-to-failure and stiffness than the RS and control groups.

Conclusion: ARS could effectively augment the tendon-to-bone integration and improve gradient microstructure in a rabbit extra-articular model by inducing the new bone formation, increasing the area of fibrocartilage, and improving collagen organization and maturation. The dual-layer aligned-random silk fibroin/P(LLA-CL) nanofibrous scaffold is proved to be a promising biomaterial for tendon-to-bone healing.

Keywords: tendon-to-bone healing, electrospinning, aligned, random, dual-layer

Introduction

Tendon/ligament injuries are common, mostly occurring during physical activity.[1] Tendon grafts such as semitendinosus, gracilis, tibialis, and peroneous longus tendons were frequently used to reconstruct the ruptured tissues.[2] Although reconstruction surgery has become increasingly popular for years, the outcomes are not always satisfactory due to the poor healing capacity of the transplanted tendons with the host tissues, especially for cases requiring enthesis regeneration.[3] Histologically, enthesis is characterized by a transitional series of tissues including tendon/ligament, fibrocartilage,

calcified fibrocartilage, and bone.[4] This distinct structure is essential for minimizing stress concentrations between the connective tissue and bone, for its gradients in mechanical properties as a natural functionally graded structure.[5]

Due to the functional significance of the enthesis, there has been a growing interest in tendon/ligament-to-bone healing. Many efforts have been made to biomimetic the structure through interfacial tissue engineering.[6] However, it is difficult to establish effective interface healing because of the complexity of the transition between soft and hard tissues. Several studies have reported that indirect connection, mostly consisting of Sharpey's-like fibers, was observed in the healing process of different tendon–bone models.[7–9] Nevertheless, this indirect connection with poorly organized fibers between the tendon and the bone was far from the native structure and had insufficient pullout strength. As a result, the inferior mechanical and biochemical properties of the repaired tissue could increase the risk of reinjury and continued disability.[10,11]

Nanofibrous scaffolds fabricated by electrospinning techniques have become increasingly popular in the field of interfacial tissue engineering in recent years.[12–14] The nanofibrous scaffolds are characterized by their good biocompatibility, high aspect ratios, and high porosity with small pore sizes.[15,16] Moreover, the morphology features of the scaffolds play an important role in cellular activity, including attachment, proliferation, and differentiation.[17,18] Yin et al[19] investigated the effects of nanotopography of electrospun scaffolds on the differentiation of human tendon stem/progenitor cells (hTSPCs) and demonstrated that the aligned scaffolds could induce the tenogenic differentiation of hTSPCs, while the random scaffolds could induce the osteogenic differentiation of hTSPCs in vitro. Zhang et al investigated the effects of nanotopography of electrospun scaffolds on the differentiation of hTSPCs-mesenchymal stem cells and demonstrated that the aligned scaffolds could induce the tenogenic differentiation of the cells, while the random scaffolds could induce the osteogenic differentiation of the cells in vitro. Besides, Yin et al[20] applied the random and aligned scaffolds in an Achilles tendon injury model in vivo and found more mature tendon-like tissues in the aligned group, while much chondrogenesis and subsequent ossification were shown in the randomly oriented group. In 2016, Park et al[21] developed a hybrid scaffold with dual configuration of aligned and random electrospun fibers for skeletal muscle tissue engineering and found that the scaffold could still influence the alignment and differentiation of the C2C12 myoblasts cells by controlling the density of aligned

layer. Recently, Liu et al[22] physically modified the tendon extracellular matrix into a random-aligned random-composite scaffold using ultrasound treatment and demonstrated that the scaffold could promote osteoinductivity in vitro and enhanced bone and fibrocartilage formation at the interface in vivo. These studies showed the possibility of modifying the scaffold for tendon-to-bone healing by integration of topographic cues.

However, so far there has been no in vivo study concerning the electrospun aligned-random scaffold (ARS) for interfacial tissue engineering. Herein, the objectives of this study were 1) to develop a dual-layer aligned-random nanofibrous scaffold by electrospinning using silk fibroin (SF)-blended poly(L-lactic acid-co-e-caprolactone) (P(LLA-CL)) and 2) to evaluate the effect of the ARS on tendon-to-bone healing in vivo, including the ability to induce tendon-to-bone integration, improve gradient microstructure, and enhance biomechanical property of the tendon in the bone tunnel, compared to the RS and control groups.

Materials and methods
Materials
Bombyx mori silkworm cocoons were generously provided by Jiaxing Silk Co. Ltd. (China). The co-polymer of P(LLA-CL) (50:50) (Mw = 34.5×10^4 g·mol^{-1}), which has a composition of 50 mol% L-lactide, was supplied by Nara Medical University (Japan). 1,1,1,3,3,3,-Hexafluoro-2-propanol (HFIP) was purchased from Daikin Industries Ltd, (Japan).

Preparation of regenerated SF
Raw silk was degummed three times with 0.5 wt% Na_2CO_3 solution (Sigma-Aldrich Co., St Louis, MO, USA) at 100°C for 0.5 h each time and then washed with sterilized distilled water three times. Degummed silk was dissolved in a ternary solvent system of $CaCl_2/H_2O$/ethanol solution (mole ratio 1/8/2) for 1 h at 70°C. After dialysis through cellulose tubular membrane (250-7u; Sigma) in distilled water for 3 days at room temperature, the SF solution was filtered and lyophilized to obtain regenerated SF sponges.

Preparation of SF/P(LLA-CL) nanofibrous scaffolds
The SF/P(LLA-CL) electrospinning solution with a concentration of 10 wt% was prepared by mixing SF and P(LLA-CL) (w/w [%] = 25:75) in HFIP and by stirring at room temperature for 5 h. The SF/P(LLA-CL) solution was fed into plastic syringe, and then the syringe was loaded in

a syringe pump (789100C; Cole-Pamer, USA) and operated at a rate of 1.2 mL/h. A high-voltage power supply of 10 kV (DW-P403-1AC-5; Dongwen Co. Ltd, China) was used. The distance between the collector and needle was 10–15 cm. The RS was fabricated. To obtain ARS, a rotating drum collector at a rate of 3,000 rpm was subsequently applied to form the aligned nanofibers on the random nanofibers. Eventually, the RS and ARS were crosslinked via alcohol vapor and placed in vacuum to remove the residual solvent.

Structural morphology of the scaffolds

The morphology of the scaffolds was observed by scanning electron microscopy (JSM-5600; Japan) at an accelerating voltage of 15 kV. The mean fiber diameters were measured using ImageJ Software (National Institutes of Health, USA).

Animal model

The animal study was approved by the Animal Research Committee of Shanghai Jiaotong University Animal Science Department. All procedures were performed following the Guide for the Care and Use of Laboratory Animals of the National Institutes of Health and the Animal Welfare Act. Ninety New Zealand white rabbits (weight, 2.8–3.2 kg;

age, 6–8 months; 30 rabbits in each group) underwent surgery to establish an extra-articular tendon-to-bone healing model with autologous Achilles tendon (Figure 1). The rabbits were anesthetized by intramuscular injection of 0.8 mL of xylazine hydrochloride and 0.8 mL of diazepam. After skin preparation, the rabbits were put supine on the operating table. An incision was made along the Achilles tendon of one hindlimb. Achilles tendon with a partial thickness of 2 cm was harvested as a graft. A bone tunnel was made in the proximal tibia of the other hindlimb at the longitudinal axis of the tibia by a 2.5-mm-diameter Kirschner wire. In the experimental group, the Achilles tendon wrapped with ARS or RS was passed through the bone tunnel, while in the control group, the unwrapped Achilles tendon was transplanted directly. Both ends of the implanted Achilles tendon were sutured to the adjacent soft tissue while the lateral end was left about 0.5 cm for future biomechanical testing. The wounds were closed layer by layer. The animals were returned to cages without immobility and they were intramuscularly injected with penicillin at a concentration of 100,000 U/kg for consecutive 3 days after surgery. The rabbits were sacrificed at 6 and 12 weeks and the graft-tibia complex (GTC) samples were harvested for the following tests.
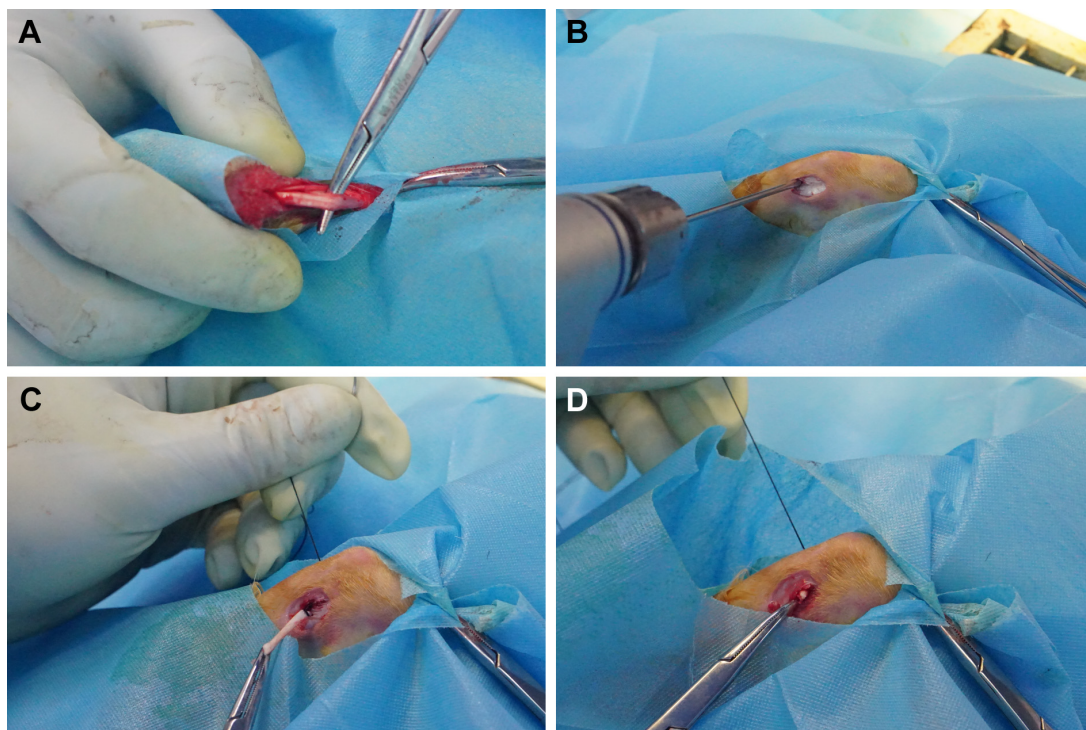

Figure 1 Animal surgery procedure.
Notes: (**A**) Partial-thickness Achilles tendon of one hindlimb was harvested. (**B**) The bone tunnel was made in the proximal tibia of the other hindlimb. (**C**, **D**) The Achilles tendon graft was passed through the bone tunnel.

Histological assessment

The GTC samples were fixed in 10% formalin, decalcified, and embedded in paraffin. Five-micrometer-thick sections were cut parallel to the long axis of the tendon and stained with hematoxylin and eosin (H&E), toluidine blue (TB), and Picrosirius red. The slides were blindly and independently evaluated by two investigators.

Metachromasia

Metachromasia is a characteristic change in the color of staining carried out in biological tissues.[23] For example, TB becomes dark blue when bound to cartilage tissues, which is considered as metachromasia. The total area of metachromasia for each sample was measured using ImageJ Software.

Interface width analysis and morphological grading

Interface width analysis and morphological grading were performed by two investigators. Briefly, three sections of each specimen were chosen and the interface width was measured as the distance between the edge of the bone tunnel and the outer tendon determined under 200× magnification. Four separate measurements were made in each section. The interface width for each specimen was determined by averaging the values obtained from each specimen. Besides, the interface tissue at the tendon–bone interface was morphologically graded according to Yamakado's classification,[24] and these grades included separation between the bone and tendon, interface without collagen fiber continuity, collagen fiber continuity, and direct type of insertion. Each group had seven specimens at each time point. If two types of interface tissues were found in the same section, then the specimen was assigned to the higher grade.

Collagen density and organization

Picrosirius red staining was used for the assessment of collagen density and organization. All sections of samples at 12 weeks were analyzed under linear polarized light at 200× magnification. Thick mature, tightly packed, and better-aligned collagen fibers were reddish-yellow, whereas thin immature fibers were green.[25,26] The areas of the two types of collagens were calculated as the average densities using the reddish-yellow fiber area/total tendon area and green fiber area/total tendon area ratios. Meanwhile, the orientation of the collagen fibers was also recorded.

Microcomputed tomography (micro-CT) analysis

At 12 weeks after surgery, the GTC samples (n = 5 in each group) were scanned perpendicular to the long-bone axis covering the entry and exit of the bone tunnel at a spatial resolution of 35 µm (1 mm aluminum filter, 65 KV, 380 µA) via Skyscan 1176 micro-CT imaging system (Bruker, Kontich, Belgium). The bone tunnel areas were measured by ImageJ Software. To quantify the amount of newly formed mineralized tissue over time, a 3.5 mm circular region of interest inside the tendon–bone tunnel was chosen and the reconstructed 3D datasets were analyzed to obtain the trabecular bone volume fraction of the total tissue volume of interest (BV/TV) value.

Biomechanical analysis

Immediately after sacrifice, the GTC samples (n = 5 in each group at each time point) were harvested and prepared for mechanical testing according to a previously reported procedure.[27] The peripheral tissues, except for the tendon graft, were carefully removed from the GTC. The biomechanical testing was performed using an electronic universal materials testing system machine (AGS-X; Shimadzu, Kyoto, Japan). The tibia was firmly fixed and the lateral end of the graft outside the bone tunnel was sutured with an Ethibond W4843 suture for traction. Before the biomechanical testing, the specimen was preloaded with a static preload of 1 N for 5 min. The ultimate failure load was carried out with an elongation rate of 2 mm/min. The load-deformation curve was recorded, from which the ultimate failure load and the stiffness were measured. For each sample, the test was completed when the graft was ruptured or pulled out of the bone tunnel.

Real-time polymerase chain reaction (RT-PCR)

The GTC samples (n = 3 in each group at each time point) were harvested after sacrifice and snap-frozen in liquid nitrogen and subsequently stored at −80°C. Total RNA from interfacial samples between graft and host bone tunnel was extracted using Trizol reagent (10296010; Invitrogen, Carlsbad, CA, USA) based on the manufacturer's instructions. The cDNA was generated using reverse-transcriptase M-MLV (D2640A; Takara Bio, Inc., Otsu, Japan) according to the manufacturer's protocol. Quantitative PCR was carried out with SYBR Premix Ex Taq (DRR041A; Takara, Beijing, China), detected by a real-time PCR system (TP800; Takara, Kyoto, Japan). Values were expressed as relative expression with respect to the endogenous control, β-actin.[28] The following primers were used for RT-PCR: β-actin, BMP-2, osteopontin (OPN), collagen I (COL I) and collagen III (COL III). Primer sequences were designed by the Primer 3 software.

Statistical analysis

Data were expressed as mean ± SD. The analysis of variance (ANOVA) and Tukey's multiple comparisons were used to determine significant differences among three groups using Graphpad Prism 7.0 statistical software. $P<0.05$ was considered to be statistically significant.

Results

Characterization of the dual-layer ARS

The cross-sectional and surface fibrous morphologies of the ARS are shown in Figure 2. The average diameters of the aligned layer and the random layer were 445 ± 180 nm and 486 ± 142 nm, respectively.

Histological assessment

Metachromasia

TB staining showed that the area of glycosaminoglycan staining at the interface between the tendon and bone was not significantly different among the three groups at 6 weeks (20,049 ± 2,696 μm^2 [ARS], 19,418 ± 2,369 μm^2 [RS], and 15,488 ± 4,236 μm^2 [control]) (Figure 3A and B). At 12 weeks, the total metachromasia area of the ARS group was significantly higher than those of the RS and control groups (61,021 ± 4,515 μm^2 [ARS], 42,184 ± 4,983 μm^2 [RS], and 33,230 ± 2,754 μm^2 [control]). Besides, significant differences were also detected between the RS and the control groups.

Interface width analysis and morphological grading

H&E staining demonstrated that there was no significant difference in terms of the interface width among the three groups at 6 weeks (Figure 3C and D) (89.8 ± 19.5 μm [ARS], 91.5 ± 20.2 μm [RS], and 93.7 ± 17.3 μm [control]). The interface width of the ARS and RS groups was much smaller than that of the control group at 12 weeks (23.2 ± 5.6 μm [ARS], 42.7 ± 8.7 μm [RS], and 83.4 ± 11.8 μm [control]). Still, no significant difference in the interface width between the ARS and RS groups was observed. Moreover, the morphological grading results for the interface tissue are shown in Table 1. Direct type of insertion could be only seen in the ARS group at 12 weeks.

Collagen type and organization

At 12 weeks, the collagen orientation of the RS and control group was not well organized (Figure 4). However, the ARS group exhibited oriented collagen fibers, the angular deviation of fibers was fairly uniform across the insertion, and the fibers
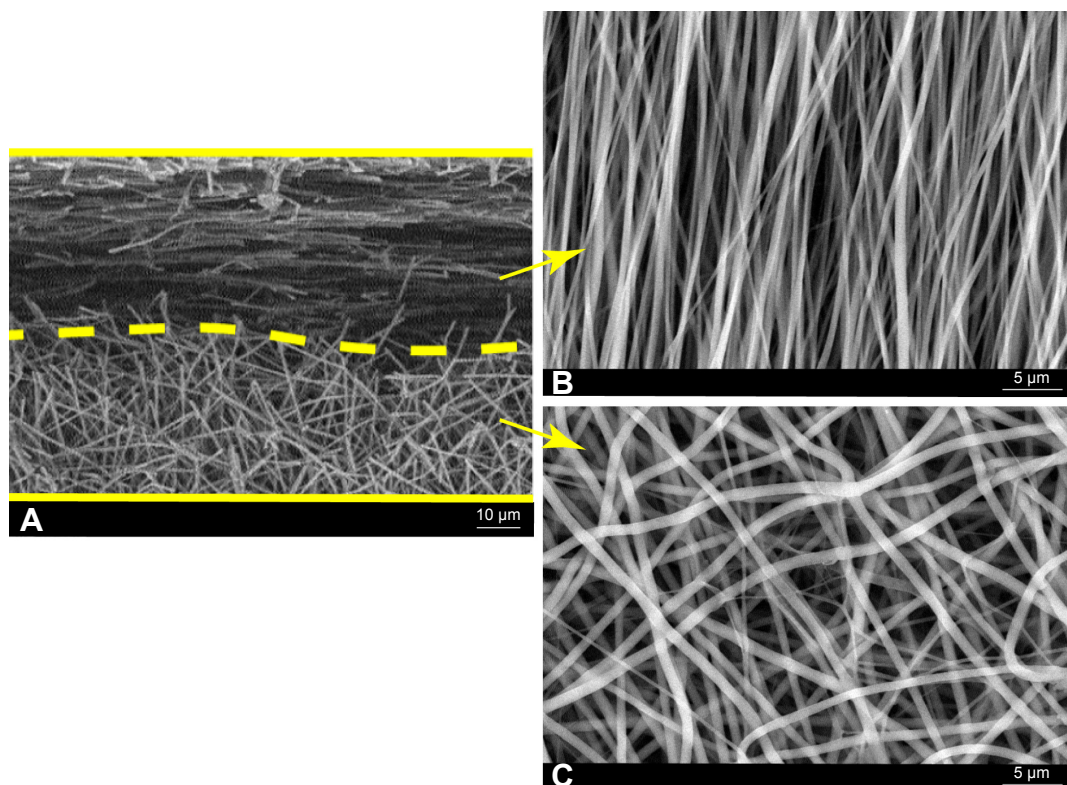

Figure 2 SEM observations of the dual-layer aligned-random nanofibrous scaffold.
Notes: (**A**) Cross-section of the scaffold; (**B**) upper layer of aligned fibers; and (**C**) lower layer of random fibers.
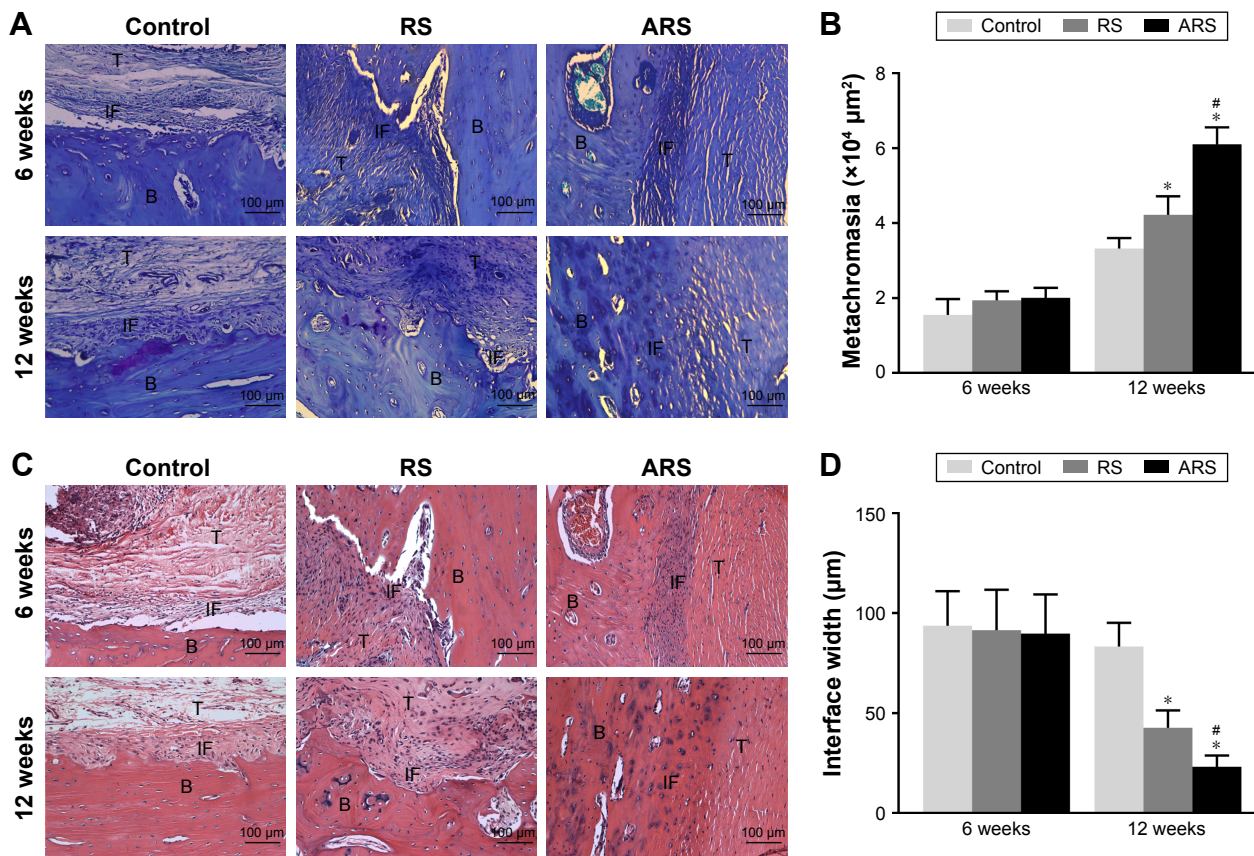**Abbreviation:** SEM, scanning electron microscopy.

Figure 3 Histological characterization of the control group, the RS group, and the ARS group at 6 and 12 weeks after surgery.
Notes: (**A**) TB staining and (**C**) H&E staining evaluation of the tendon–bone interface at 6 weeks after surgery. (**B**) Metachromasia analysis with TB-stained slides. Higer level of metachromasia indicates more mature fibrocartilage. (**D**) Interface width analysis with H&E-stained slides. *$P < 0.05$ vs control, #$P < 0.05$ vs RS group. Smaller interface width indicates better osteointegration to the tendon.
Abbreviations: B, bone; IF, interface; T, tendon; RS, random scaffold; ARS, aligned-random scaffold; H&E, hematoxylin and eosin.

were anchoring closely to the bone. The reddish-yellow fiber area/total tendon area ratio of ARS group was significantly higher than those of the RS and control groups ($50.6\% \pm 1.7\%$ [ARS], $8.9\% \pm 0.9\%$ [RS], and $7.4\% \pm 1.1\%$ [control]), while the green fiber area/total tendon area ratio was significantly lower than those of the RS and control groups ($5.3\% \pm 0.7\%$ [ARS], $48.2\% \pm 4.1\%$ [RS], and $53.3\% \pm 3.7\%$ [control]).

Micro-CT analysis

New bone formation was observed at the interface between the tendon and tibial bone tunnel in all the three groups at

12 weeks (Figure 5). The RS and ARS groups showed higher new bone formation compared with the control group. The BT/TV value of the RS and ARS groups was significantly higher than that of the control group at 12 weeks ($9.0\% \pm 0.9\%$ [ARS], $9.2\% \pm 0.7\%$ [RS], and $5.2\% \pm 1.4\%$ [control]). The BT/TV value between the RS and ARS groups was not significantly different. Accordingly, the average bone tunnel area of the RS and ARS groups was significantly smaller than that of the control group ($3.8 \pm 0.3 \, mm^2$ [ARS], $3.8 \pm 0.3 \, mm^2$ [RS], and $4.7 \pm 0.5 \, mm^2$ [control]). However, there was no significant difference between RS and ARS groups.

Biomechanical testing

All grafts were pulled out from the bone and no graft rupture occurred. The ultimate failure load and stiffness increased in all the three groups from 6 to 12 weeks after surgery (Figure 6). At 6 weeks, the ultimate failure load of the ARS and the RS groups was higher than that of the control group, respectively ($43.9 \pm 7.5 \, N$ [ARS], $41.4 \pm 5.7 \, N$ [RS], and $25.3 \pm 5.9 \, N$ [control]). However, significant difference was not detected between the ARS and the RS groups until

Table 1 Yamakado interface morphological grade

	6 weeks (n = 7)			12 weeks (n = 7)		
	Control	RS	ARS	Control	RS	ARS
Direct type of insertion	0	0	0	0	0	2
Collagen–fiber continuity	0	0	4	3	3	5
Interface without fiber continuity	3	4	2	3	4	0
Separation	4	3	1	1	0	0

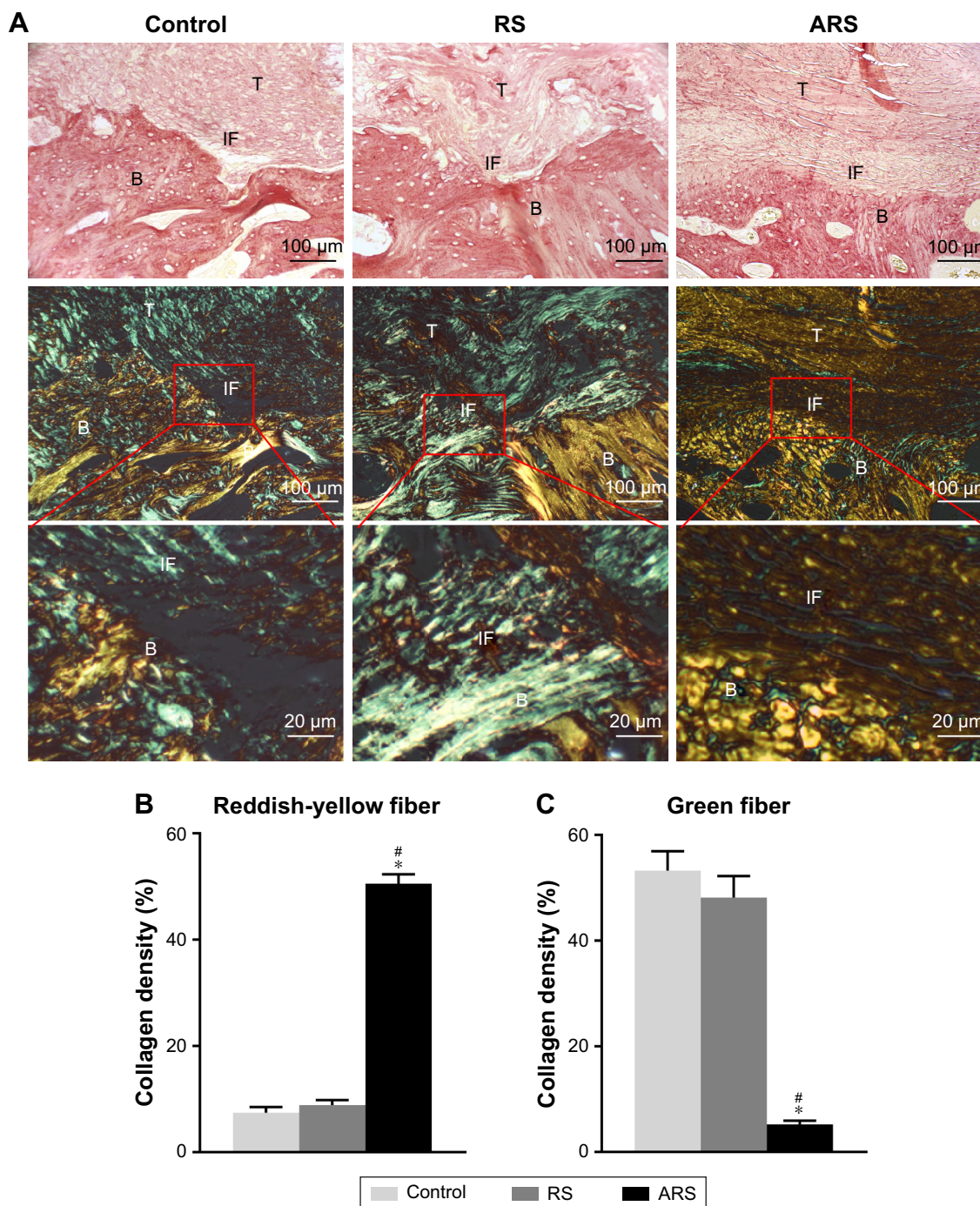**Abbreviations:** RS, random scaffold; ARS, aligned-random scaffold.

Figure 4 Results of Picrosirius red staining evaluation of the control group, the RS group, and the ARS group at 12 weeks after surgery.
Notes: (**A**) Images observed under normal condition are shown on the first row. Corresponding sections observed under polarizing condition are shown on the second row. Partial magnifications of the red rectangle area are displayed on the third row. Collagen density analysis includes the reddish-yellow fiber area/total tendon area ratio (**B**) and the green fiber area/total tendon area ratio (**C**). The collagen fibers are most mature in the ARS group at 12 weeks after surgery. $*P<0.05$ vs control, $\#P<0.05$ vs RS group.
Abbreviations: T, tendon; B, bone; IF, interface; RS, random scaffold; ARS, aligned-random scaffold.

at 12 weeks (83.2 ± 12.4 N [ARS], 66.2 ± 6.6 N [RS], and 50.6 ± 3.5 N [control]). Similarly, the stiffness of the ARS and the RS groups was significantly higher than that of the control group at 6 weeks (9.9 ± 1.9 N/mm [ARS], 9.3 ± 1.4 N/mm [RS], and 5.8 ± 1.3 N/mm [control]). At 12 weeks, there was significantly higher stiffness in the ARS group than in the

RS group (21.5 ± 3.5 N/mm [ARS], 15.6 ± 1.6 N/mm [RS], and 10.0 ± 1.1 N/mm [control]).

RT-PCR
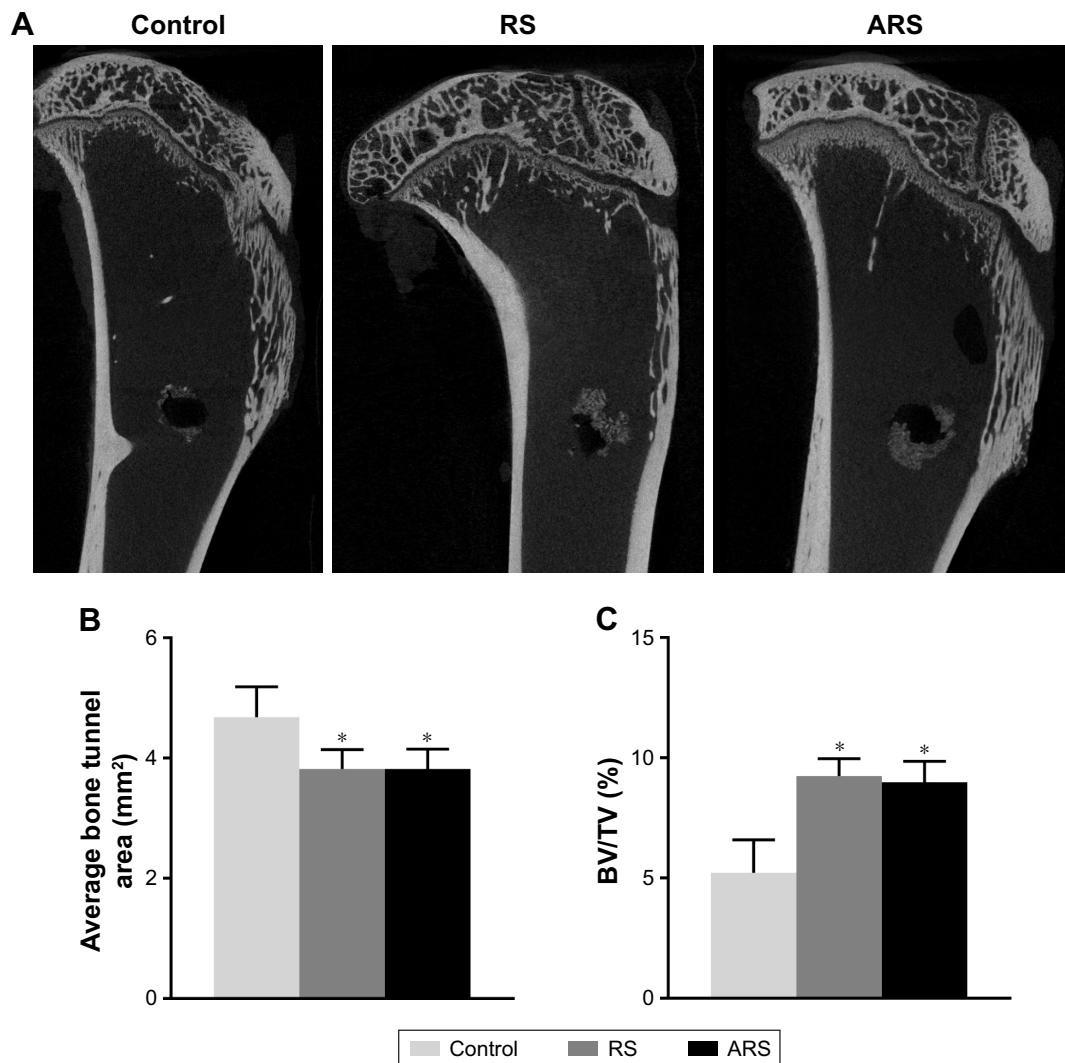At 6 weeks, BMP-2 and OPN expression levels of the RS and ARS groups were higher than those of the control group,

Figure 5 Micro-CT analysis of the control group, the RS group, and the ARS group at 12 weeks after surgery.
Notes: (**A**) Micro-CT scans of the specimens of three groups at 12 weeks after surgery. (**B**) Quantification of the average bone tunnel area. (**C**) The BV/TV value. Smaller bone tunnel area and higher BV/TV value indicate higher new bone formation. $*P < 0.05$ vs control.
Abbreviations: micro-CT, microcomputed tomography; BV/TV, trabecular bone volume fraction of the total tissue volume; RS, random scaffold; ARS, aligned-random scaffold.

respectively (Figure 7). However, difference was not detected between the two groups. At 12 weeks, BMP-2 and OPN expression levels showed no significant difference among the three groups. Moreover, collagen I expression level of the ARS group was significantly higher than those of the RS and control groups at 6 and 12 weeks, respectively, while collagen III expression level of the ARS group was significantly lower than those of the RS and control groups at 6 and 12 weeks, respectively. However, neither collagen I nor collagen III expression levels showed significant difference between the RS and control groups.

Discussion

According to the previous studies, SF has good biocompatibility and potential osteogenic induction.[29] It is demonstrated

that the random SF nanofibrous scaffold could accelerate MC3T3-E1 cells proliferation and osteogenic differentiation in vitro and promote new bone formation in vivo as well.[30,31] Moreover, Vaquette et al[32] found that bone marrow mesenchymal stem cells could spontaneously orientate along the microfibers and produce collagen I and III on the aligned P(LLA-CL) mat, making the seeded scaffolds similar to ligaments in morphology. However, the effect of SF/P(LLA-CL) materials on tendon-to-bone healing remains unclear. In this study, we fabricated SF-blended P(LLA-CL) nanofibrous scaffolds and investigated their effect on tendon-to-bone healing.

The micro-CT images showed that new bone formation was observed at the interface in the RS and ARS groups. The BV/TV value of the RS and ARS groups was also higher
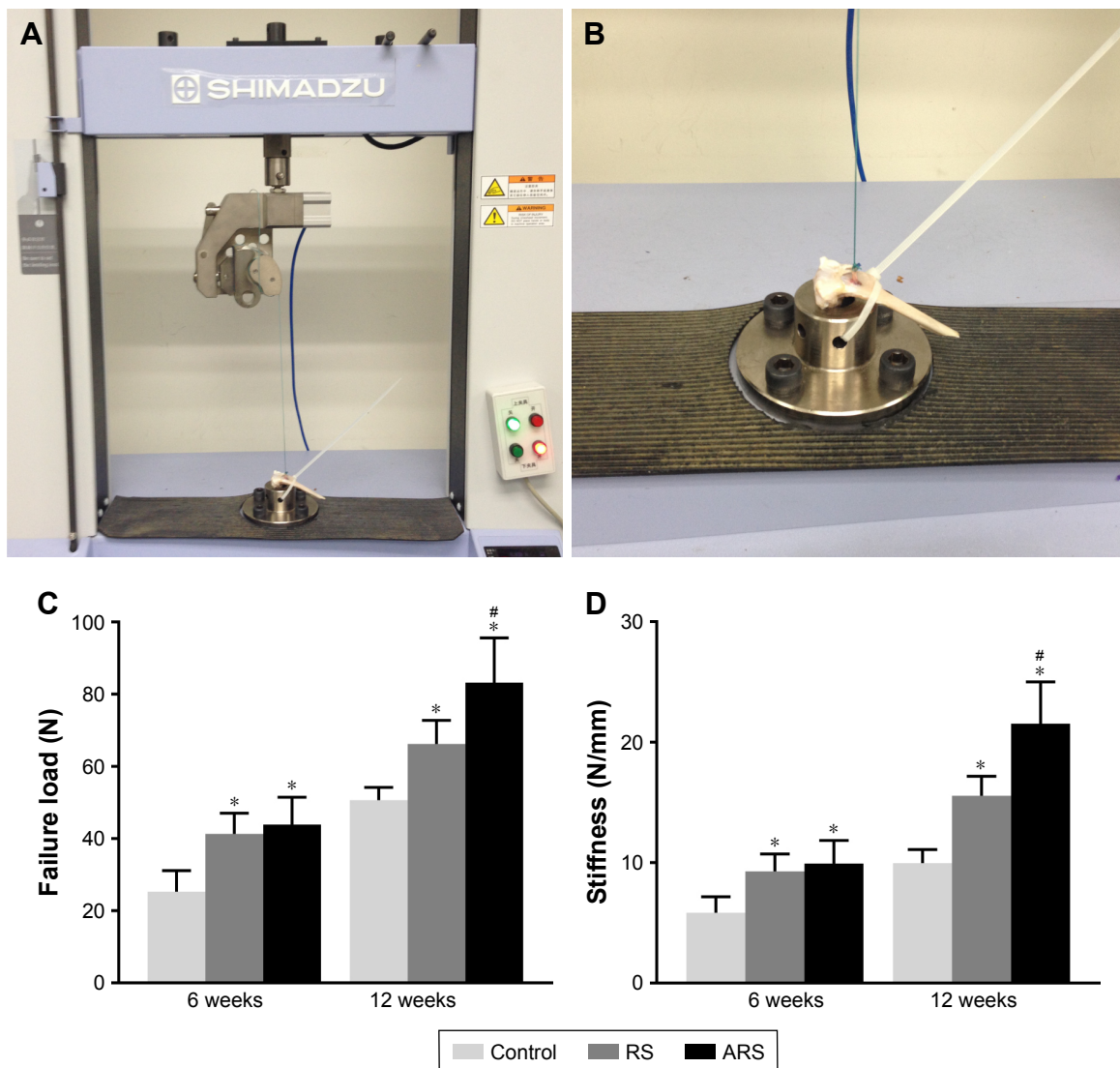
Figure 6 Biomechanical testing for tendon-to-bone healing of the control group, the RS group, and the ARS group at 6 and 12 weeks after surgery.
Notes: (**A**, **B**) Digital camera image of biomechanical test experiment of implanted graft. Red arrow points to the graft. (**C**) Comparison of the maximal failure load among the three groups. (**D**) Comparison of the stiffness among the three groups. The ARS group showed best biomechanical property at 6 and 12 weeks after surgery. *$P<0.05$ vs control, #$P<0.05$ vs RS group.
Abbreviations: RS, random scaffold; ARS, aligned-random scaffold.

than that of the control group. This was consistent with the histological result that the interface width of the RS and ARS groups was smaller than that of the control group. More new bone formation at the tendon–bone interface indicated lower interface width.[11] Moreover, RT-PCR showed that the expression levels of BMP-2 and OPN, the important osteogenic markers, were higher in the RS and ARS groups than those in the control group at 6 weeks. BMP-2 was found at the interface between the tendon and bone throughout the 12-week study period in a rabbit model and was found to be associated with bone and cartilage formation.[33,34] Moreover, it was reported that BMP-2 could act via the Ras-mitogen-activated protein kinase signaling pathway, which ultimately

leads to OPN, alkaline phosphatase, and osteocalcin expression in the osteoblasts.[35] Our results indicated that there was stronger induction of bone formation in the RS and ARS groups, which is favorable for the enthesis formation. We speculated that two factors were associated with the bone formation. On the one hand, SF was regarded as a favorable scaffold material for bone formation due to its ability to support the differentiation of mesenchymal stem cells along the osteogenic lineage via different pathways.[29,36] On the other hand, the random nanotopography of the scaffold could induce stem cells to differentiate into osteogenic lineage.[20,37] Wang et al[38] applied the random SF/P(LLA-CL) nanofibrous scaffold to bone tissue engineering and found
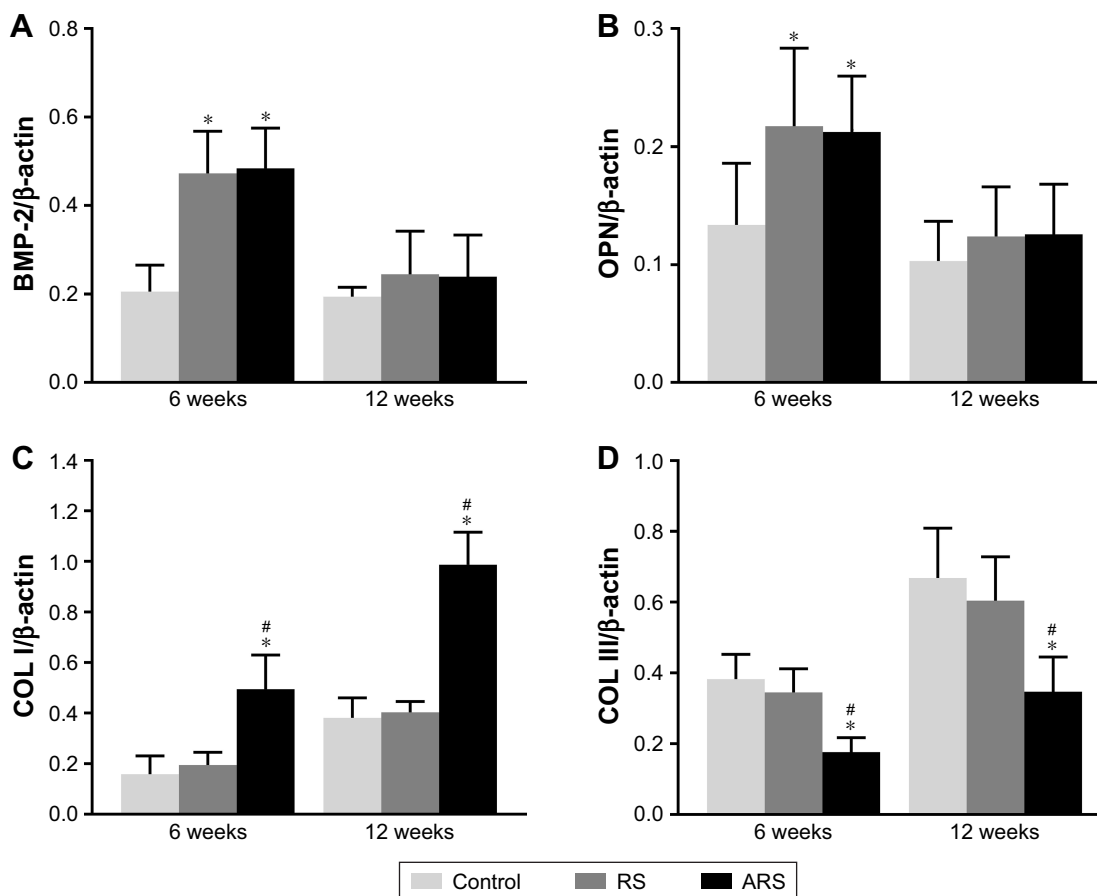
Figure 7 Comparison of the relative mRNA expression of individual genes at the interfacial tissue between graft and host bone of the control group, the RS group, and the ARS group at 6 and 12 weeks after surgery.
Notes: Comparison of the relative mRNA expression of BMP-2 (**A**), OPN (**B**), COL I (**C**), and COL III (**D**) at 6 and 12 weeks among the three groups. BMP-2 and OPN indicate the osteogenic level, and COL I and COL III indicate the mature level of collagen fibers. *$P<0.05$ vs control, #$P<0.05$ vs RS group.
Abbreviations: BMP-2, bone morphogenetic protein 2; OPN, osteopontin; COL I, collagen I; COL III, collagen III; RS, random scaffold; ARS, aligned-random scaffold.

that the scaffold could facilitate human adipose-derived stem cells (hASCs) osteogenic differentiation and promote new bone formation in a calvarial defect model of rats. This study also illustrated the osteogenesis ability of the random SF/P(LLA-CL) scaffold.

Moreover, based on the histological results of our study, the ARS implanted in vivo could effectively improve the histological structure of the tendon-to-bone area after surgery. It is believed that multilayer materials are very suitable for the interfacial tissue engineering, for they can make full use of the properties of different layers and form the grading structure, which are similar to the native enthesis.[39] We applied the dual-layer aligned-random nanofibrous scaffold in order to further improve not only the bone tissue formation but also the alignment of the collagen fiber, thus mimicking the structure of the native four zones including tendon, fibrocartilage, calcified fibrocartilage, and bone, for the tendon-to-bone healing. Generally, the collagen fibers between the tendon and bone progressively reorganized

and matured during the tendon-to-bone healing process.[40,41] Orr et al[42] demonstrated that aligned electrospun scaffold could increase the expression of tenomodulin compared to nonaligned scaffolds and exhibited aligned collagen fibrils throughout the full thickness following seeding with hASCs for 28 days in vitro. In the present study, the in vivo experiment also showed that the collagen fibers at the interface between the tendon and bone were oriented in the ARS group at 6 weeks. At 12 weeks, the fibers deviated mildly but were fairly uniform and continuous. This may be caused by the bone-tendon contact stress. Besides, the collagen fibers of the ARS group also showed the highest reddish-yellow fiber area/total tendon area ratio as compared with the other two groups at 12 weeks, which indicated the highest level of maturation among the three groups. The expression levels of collagen I and collagen III indicated the composition of the collagen fibers. The histological finding was in accordance with the RT-PCR results that the collagen I levels in the ARS group were the highest among the three groups. More importantly,

direct type of insertion, consisting of four zones, could be only seen in the ARS group at 12 weeks.

However, re-establishment of the direct attachment at the interface without any biological strategies was not easy. Rodeo et al[40] reported that direct type of tendon-to-bone healing could not be seen in a dog extra-articular model during 26 weeks after surgery. Newsham-West et al[43] investigated the process of tendon–bone healing after patellar tendon re-attachment surgery in a sheep model and found that the interface between the tendon and bone was still hypercellular and no layer of fibrocartilage tissue was observed after 104 weeks. Based on the Yamakado Interface Morphological Grade, direct type of insertion could be only seen in the ARS group at 12 weeks in our study. Moreover, according to the metachromasia analysis, significant differences were detected among the three groups, with the total metachromasia area of the ARS group being the highest. As intense metachromatic staining with TB was considered an indicator of mature fibrocartilage formation,[44] we believe that combination of aligned and random morphology of the scaffold could facilitate the organization and maturation of collagen fibers as well as the fibrocartilage chondroid formation at the interface.

Actually, the final purpose of satisfactory tendon-to-bone healing is to enhance the biomechanical property of the tendon in the bone tunnel. In our study, the higher ultimate failure load and stiffness of the ARS and the RS groups were attributed to the random morphology of the SF/P(LLA-CL) material in the RS and ARS groups, which could induce and augment bone ingrowth into the interface, thus helping to improve biomechanical property of the tendon–bone tissues. At 12 weeks, there were significantly higher ultimate failure load and stiffness in the ARS group than in the RS group, which was consistent with the histological results. The interface between the bone and the tendon in the ARS group had more mature structure than other groups at 12 weeks. Especially, direct type of insertion was only seen in the ARS group, which could afford effective transfer of mechanical loads between soft tissue and hard tissue and enhance the biomechanical property of the tendon-to-bone structure remarkably.[45] Chronologically, the progressive increase in biomechanical property was correlated with the degree of bone ingrowth, mineralization, and maturation of the healing tissue according to the histology.[40]

This study has two limitations. First, the tendon-to-bone healing model used in this study differs from that used in humans. However, this animal model has been well established in the literatures.[27,46] Second, this is a pilot study with a small sample size, and the observation period and evaluation tools are limited. However, the differences are statistically significant among the groups, and the results are encouraging. Our study offers a novel biologic approach to enhance the tendon–bone healing of soft tissue graft with the dual-layer aligned-random SF/P(LLA-CL) nanofibrous scaffold.

Conclusion

ARS could effectively augment the tendon-to-bone integration and improve gradient microstructure in a rabbit extra-articular model by inducing new bone formation, increasing the area of fibrocartilage, and improving collagen organization and maturation. This positive effect comes from both the two layers of the scaffold. Therefore, the dual-layer aligned-random SF/P(LLA-CL) nanofibrous scaffold is proved to be a promising biomaterial for tendon-to-bone healing. Intra-articular ligament reconstruction using this material in a big animal is needed for further evaluation.

Acknowledgments

Disclosure

The authors report no conflicts of interest in this work.

References

1. September AV, Schwellnus MP, Collins M. Tendon and ligament injuries: the genetic component. *Br J Sports Med*. 2007;41(4):241–246; discussion 246.
2. Sherman SL, Chalmers PN, Yanke AB, et al. Graft tensioning during knee ligament reconstruction: principles and practice. *J Am Acad Orthop Surg*. 2012;20(10):633–645.
3. Milz S, Rufai A, Buettner A, Putz R, Ralphs JR, Benjamin M. Three-dimensional reconstructions of the Achilles tendon insertion in man. *J Anat*. 2002;200(Pt 2):145–152.
4. Lu HH, Thomopoulos S. Functional attachment of soft tissues to bone: development, healing, and tissue engineering. *Annu Rev Biomed Eng*. 2013;15(1):201–226.
5. Liu YX, Thomopoulos S, Birman V, Li JS, Genin GM. Bi-material attachment through a compliant interfacial system at the tendon-to-bone insertion site. *Mech Mater*. 2012;49(1):83–92.
6. Paxton JZ. Current progress in enthesis repair: strategies for interfacial tissue engineering. *Orthop Muscular Syst*. 2012;S1:003.
7. Tabuchi K, Soejima T, Kanazawa T, Noguchi K, Nagata K. Chronological changes in the collagen-type composition at tendon-bone interface in rabbits. *Bone Joint Res*. 2012;1(9):218–224.
8. Van Kampen C, Arnoczky S, Parks P, et al. Tissue-engineered augmentation of a rotator cuff tendon using a reconstituted collagen scaffold: a histological evaluation in sheep. *Muscles Ligaments Tendons J*. 2013;3(3):229–235.

9. Kawakami Y, Takayama K, Matsumoto T, et al. Anterior cruciate ligament-derived stem cells transduced with BMP2 accelerate graft-bone integration after ACL reconstruction. *Am J Sports Med*. 2017;45(3):584–597.

10. Rothrauff BB, Tuan RS. Cellular therapy in bone-tendon interface regeneration. *Organogenesis*. 2014;10(1):13–28.

11. Atesok K, Fu FH, Wolf MR, et al. Augmentation of tendon-to-bone healing. *J Bone Joint Surg Am*. 2014;96(6):513–521.

12. Zhao S, Zhao J, Dong S, et al. Biological augmentation of rotator cuff repair using bFGF-loaded electrospun poly(lactide-co-glycolide) fibrous membranes. *Int J Nanomedicine*. 2014;9:2373–2385.

13. Han F, Zhang P, Sun Y, Lin C, Zhao P, Chen J. Hydroxyapatite-doped polycaprolactone nanofiber membrane improves tendon-bone interface healing for anterior cruciate ligament reconstruction. *Int J Nanomedicine*. 2015;10:7333–7343.

14. Sun YY, Han F, Zhang P, et al. A synthetic bridging patch of modified co-electrospun dual nano-scaffolds for massive rotator cuff tear. *J Mater Chem B*. 2016;4(45):7259–7269.

15. Zhang K, Wang H, Huang C, Su Y, Mo X, Ikada Y. Fabrication of silk fibroin blended P(LLA-CL) nanofibrous scaffolds for tissue engineering. *J Biomed Mater Res A*. 2010;93(3):984–993.

16. Chen M, Patra PK, Lovett ML, Kaplan DL, Bhowmick S. Role of electrospun fibre diameter and corresponding specific surface area (SSA) on cell attachment. *J Tissue Eng Regen Med*. 2009;3(4):269–279.

17. Huang CY, Hu KH, Wei ZH. Comparison of cell behavior on pva/pva-gelatin electrospun nanofibers with random and aligned configuration. *Sci Rep*. 2016;6:37960.

18. Mahmoodinia Maymand M, Soleimanpour-Lichaei HR, Ardeshirylajimi A, et al. Improvement of hepatogenic differentiation of iPS cells on an aligned polyethersulfone compared to random nanofibers. *Artif Cells Nanomed Biotechnol*. 2018;46(4):853–860.

19. Yin Z, Chen X, Chen JL, et al. The regulation of tendon stem cell differentiation by the alignment of nanofibers. *Biomaterials*. 2010;31(8):2163–2175.

20. Yin Z, Chen X, Song HX, et al. Electrospun scaffolds for multiple tissues regeneration in vivo through topography dependent induction of lineage specific differentiation. *Biomaterials*. 2015;44:173–185.

21. Park SH, Kim MS, Lee B, et al. Creation of a hybrid scaffold with dual configuration of aligned and random electrospun fibers. *ACS Appl Mater Interfaces*. 2016;8(4):2826–2832.

22. Liu H, Yang L, Zhang E, et al. Biomimetic tendon extracellular matrix composite gradient scaffold enhances ligament-to-bone junction reconstruction. *Acta Biomater*. 2017;56:129–140.

23. Bergeron JA, Singer M. Metachromasy: an experimental and theoretical reevaluation. *J Biophys Biochem Cytol*. 1958;4(4):433–457.

24. Yamakado K, Kitaoka K, Yamada H, Hashiba K, Nakamura R, Tomita K. The influence of mechanical stress on graft healing in a bone tunnel. *Arthroscopy*. 2002;18(1):82–90.

25. Xie Y, Chen J, Han P, Yang P, Hou J, Kang YJ. Immunohistochemical detection of differentially localized up-regulation of lysyl oxidase and down-regulation of matrix metalloproteinase-1 in rhesus monkey model of chronic myocardial infarction. *Exp Biol Med*. 2012;237(7):853–859.

26. Wågsäter D, Paloschi V, Hanemaaijer R, et al. Impaired collagen biosynthesis and cross-linking in aorta of patients with bicuspid aortic valve. *J Am Heart Assoc*. 2013;2(1):e000034.

27. Zhi Y, Wen L, Peng Z, Jia J, Chen S. Electrospun silk fibroin mat enhances tendon-bone healing in a rabbit extra-articular model. *Biotechnol Lett*. 2016;38(10):1–9.

28. Joshi S, Clapp WL, Wang W, Khan SR. Osteogenic changes in kidneys of hyperoxaluric rats. *Biochim Biophys Acta*. 2015;1852(9):2000–2012.

29. Midha S, Murab S, Ghosh S. Osteogenic signaling on silk-based matrices. *Biomaterials*. 2016;97:133–153.

30. Kim KH, Jeong L, Park HN, et al. Biological efficacy of silk fibroin nanofiber membranes for guided bone regeneration. *J Biotechnol*. 2005;120(3):327–339.

31. Meechaisue C, Wutticharoenmongkol P, Waraput R, et al. Preparation of electrospun silk fibroin fiber mats as bone scaffolds: a preliminary study. *Biomed Mater*. 2007;2(3):181–188.

32. Vaquette C, Kahn C, Frochot C, et al. Aligned poly(L-lactic-co-e-caprolactone) electrospun microfibers and knitted structure: a novel composite scaffold for ligament tissue engineering. *J Biomed Mater Res A*. 2010;94(4):1270–1282.

33. Kohno T, Ishibashi Y, Tsuda E, Kusumi T, Tanaka M, Toh S. Immunohistochemical demonstration of growth factors at the tendon-bone interface in anterior cruciate ligament reconstruction using a rabbit model. *J Orthop Sci*. 2007;12(1):67–73.

34. Chen D, Zhao M, Mundy GR. Bone morphogenetic proteins. *Growth Factors*. 2004;22(4):233–241.

35. Haversath M, Catelas I, Li X, Tassemeier T, Jager M. PGE(2) and BMP-2 in bone and cartilage metabolism: 2 intertwining pathways. *Can J Physiol Pharmacol*. 2012;90(11):1434–1445.

36. Melke J, Midha S, Ghosh S, Ito K, Hofmann S. Silk fibroin as biomaterial for bone tissue engineering. *Acta Biomater*. 2016;31:1–16.

37. Dalby MJ, Gadegaard N, Tare R, et al. The control of human mesenchymal cell differentiation using nanoscale symmetry and disorder. *Nat Mater*. 2007;6(12):997–1003.

38. Wang Z, Lin M, Xie Q, et al. Electrospun silk fibroin/poly(lactide-co-epsilon-caprolactone) nanofibrous scaffolds for bone regeneration. *Int J Nanomedicine*. 2016;11:1483–1500.

39. Kim BS, Kim EJ, Choi JS, Jeong JH, Jo CH, Cho YW. Human collagen-based multilayer scaffolds for tendon-to-bone interface tissue engineering. *J Biomed Mater Res A*. 2014;102(11):4044–4054.

40. Rodeo SA, Arnoczky SP, Torzilli PA, Hidaka C, Warren RF. Tendon-healing in a bone tunnel. A biomechanical and histological study in the dog. *J Bone Joint Surg Am*. 1993;75(12):1795–1803.

41. Weiler A, Hoffmann RF, Bail HJ, Rehm O, Sudkamp NP. Tendon healing in a bone tunnel. Part II: histologic analysis after biodegradable interference fit fixation in a model of anterior cruciate ligament reconstruction in sheep. *Arthroscopy*. 2002;18(2):124–135.

42. Orr SB, Chainani A, Hippensteel KJ, et al. Aligned multilayered electrospun scaffolds for rotator cuff tendon tissue engineering. *Acta Biomater*. 2015;24:117–126.

43. Newsham-West R, Nicholson H, Walton M, Milburn P. Long-term morphology of a healing bone-tendon interface: a histological observation in the sheep model. *J Anat*. 2007;210(3):318–327.

44. Weischer CH, Krisinger J, Karzel K. Effects of mellitic acid (MA) and sodium fluoride (NaF) on the histological appearance of murine fetal tibiae cultured in vitro. *Histol Histopathol*. 1986;1(3):303–308.

45. Li X, Xie J, Lipner J, Yuan X, Thomopoulos S, Xia Y. Nanofiber scaffolds with gradations in mineral content for mimicking the tendon-to-bone insertion site. *Nano Lett*. 2009;9(7):2763.

46. Zhang P, Zhi Y, Fang H, et al. Effects of polyvinylpyrrolidone-iodine on tendon-bone healing in a rabbit extra-articular model. *Exp Ther Med*. 2017;13(6):2751–2756.